mater.scichina.com link.springer.com

Published online 14 December 2022 | https://doi.org/10.1007/s40843-022-2271-2
Sci China Mater 2023, 66(4): 1649–1658

Back stress dynamic balancing strategy enabled strength-ductility synergy in heterostructured Al-SiC composites

Dongxin Mao[1†], Xiangchen Meng[1,2†], Yuming Xie[1,2†], Yuexin Chang[1], Zhiwei Qin[1], Shuangming Xu[3], Long Wan[1] and Yongxian Huang[1,2*]

ABSTRACT Strength-ductility trade-off dilemma remains a significant obstacle to high-strength composites due to the undesirable dislocation storability. Herein, an ingenious nano-micro SiC-reinforced Al matrix composite (AMC) with heterogeneous grain structures of coarse and fine grains was designed *via* a novel deformation-driven metallurgy method. The accumulated geometrically necessary dislocations and the intragranularly dispersed SiC particles were tailored based on the principle of back stress amelioration, which was a key point to maintain the dynamic balance with the applied stress toward strength-ductility synergy. The ultimate tensile strength and uniform elongation of the designed $SiC_{5np\text{-}5\mu p}$/Al composite reached 324 MPa and 12.9%, respectively, and the strength was 181% as high as that of the $SiC_{10\mu p}$/Al with only 3% ductility loss. As such, a new strategy was provided herein to promote strength-ductility synergy *via* the further modified back stress.

Keywords: aluminum matrix composites, deformation-driven metallurgy, heterostructures, back stress, strength-ductility synergy

INTRODUCTION

Aluminum matrix composites (AMCs) reinforced with ceramic particles, carbon nanotubes, or graphene, as lightweight structural materials, have wide applications in the aerospace and military industries [1–3]. Especially for the SiC particles, the reinforced AMCs have attracted great attention for their low costs and high strengthening efficiency [4–6], and have been widely used in spacecraft such as the dual-axis antenna drive mechanism in the Zhurong rover. In consideration of the strict service conditions of aerospace and military, AMCs are required to be lighter, stronger, and more ductile [7–9]. However, the high strength of the reinforced AMCs is usually at the expense of a considerable ductility loss, as the grains refined by SiC particles have a low dislocation storability [10]. A major challenge for the AMCs is to achieve a desirable strength-ductility synergy [11–13].

Designing heterogeneous structures in AMCs to introduce back stress strengthening is an effective way to evade the strength-ductility trade-off [11,12,14]. A kind of typical heterogeneous AMC contains grains of different sizes [15,16]. The regions with fine or coarse grains are considered as the hard-brittle zones and the soft-ductile zones, which undertake the role of strengthening and straining, respectively [17]. During the tensile deformation, geometrically necessary dislocations (GNDs) would be induced between the two zones, leading to an extra-strengthening, namely back stress strengthening [18]. The stress partitioning and strain transfer are procured during the deformation process. The yield strengths of these AMCs exceed the prediction simply by the rule-of-mixture [19]. The characteristic of such a strengthening mechanism is that the soft-ductile zones provide enough space for the dislocations to glide, which promotes accommodating strain incompatibility. The structure or the proportion of the hard-brittle zones and the soft-ductile zones are usually modified to enhance the strengthening efficiency [20]. In AMCs with much more soft-ductile zones, GNDs may glide relatively freely, as less hindered by the surrounding hard-brittle zones. Such freely-glide GNDs are not beneficial to the strength improvement, although the ductile feature may be kept. As such, a strategy to design heterogeneous materials is necessary to further strengthen the back stress and then promote strength-ductility synergy.

The materials with random mixtures of coarse and fine grains have a strength-ductility trade-off dilemma [21]. In the present work, the intragranularly dispersed SiC reinforcements were introduced into the random mixed coarse-fine grain structures in the SiC-reinforced AMCs to promote back stress strengthening, as the intragranularly dispersed reinforcements could increase the back stress through the load sharing or the dislocations-particles short range interaction [22–24]. The increased back stress was desired to keep the dynamic balance with the accumulated applied stress, which was the key point to maintaining the strength-ductility synergy. The design principles of the heterogeneous structure with enhanced strength-ductility are shown in Fig. 1. A novel solid severe plastic deformation method, namely deformation-driven metallurgy (DDM), was utilized to prepare the designed structure. The heterogeneous structure formation and its strength-ductility synergy mechanism were clarified in detail. An effective strategy and a theoretical basis were provided to overcome the strength-

[1] State Key Laboratory of Advanced Welding and Joining, Harbin Institute of Technology, Harbin 150001, China
[2] Zhengzhou Research Institute, Harbin Institute of Technology, Zhengzhou 450000, China
[3] China Aerospace Science and Technology Corporation, Beijing 100000, China
[†] These authors contributed equally to this work.
[*] Corresponding author (email: yxhuang@hit.edu.cn)

 © Science China Press and Springer-Verlag GmbH Germany, part of Springer Nature 2022

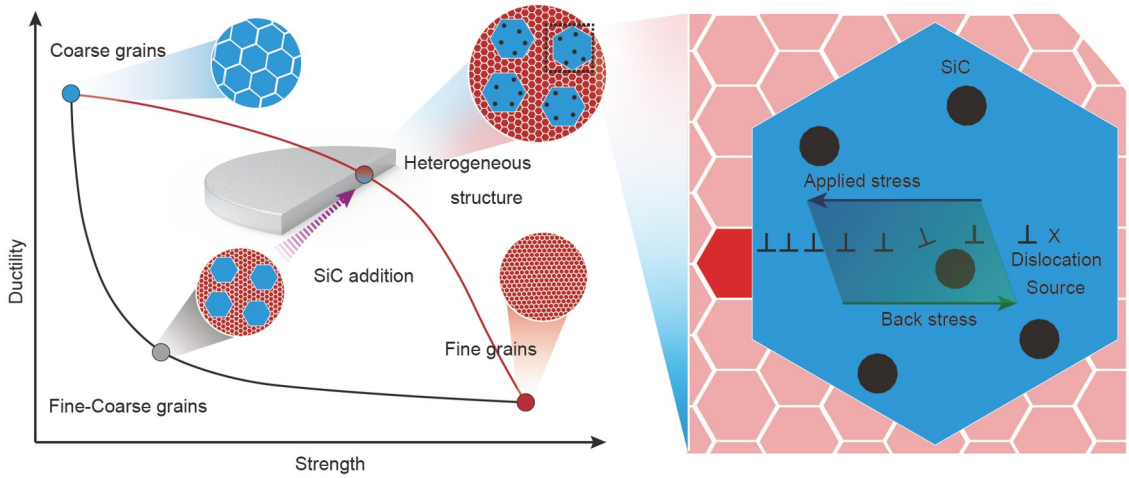

Figure 1 Design principles of the strength-ductility synergy of the SiC-reinforced AMCs.

ductility trade-off dilemma.

EXPERIMENTAL SECTION

Spherical 1060 pure aluminum (Al) powders (purity > 99.6%) with an average diameter of 5 μm were utilized as the matrix. The exact composition of the 1060 pure Al was given in Table S1. The 10 wt% mixed SiC particles containing nano-SiC particles (SiC_{np}, 10 nm in average diameter, purity > 99.0%) and micro-SiC particles ($SiC_{\mu p}$, 2 μm in average diameter, purity > 99.0%) were added to reinforce the matrix. Two types of mixed SiC particles with different proportions were prepared with mass ratios of nano-SiC particles to micro-SiC particles being 7:3 and 5:5, respectively. Pure Al powders reinforced by 10 wt% micro-SiC particles or 10 wt% nano-SiC particles served as the control groups. The four sets of samples were named SiC_{10np}/Al, $SiC_{7np\text{-}3\mu p}$/Al, $SiC_{5np\text{-}5\mu p}$/Al, and $SiC_{10\mu p}$/Al, respectively. The SiC and Al powders were blended by a planetary ball milling machine at a rotational velocity of 200 r min^{-1} for 10 h. The ball-to-powder ratio and the size of the milling ball (ZrO_2) were 5:1 and 6 mm, respectively. Fig. S1 depicts that both nano-SiC and micro-SiC particles were mixed with the Al powders uniformly. The image of raw nano-SiC particles was also given in Fig. S1a. Especially, the aggregation tendency of nano-SiC particles with a large surface-to-volume ratio was alleviated, making them distributed homogeneously over the surface of the Al powders (Fig. S1c). The milled powders were pre-compacted at 200 MPa for 60 s by a cold tubular mold. Then, the round preform was placed in the Al mold and was sheared and stirred by a processing tool for 30 s with a rotational velocity of 800 r min^{-1}. The compaction ratio was set as 2:1. As shown in Fig. 2, a perfect Al composite disc reinforced by the SiC particles was achieved following the specific three steps. The detailed schematic of the whole preparation process was given in Fig. S2.

The morphologies of the raw powders and composites were characterized by scanning electron microscope (SEM) at a working voltage of 20 kV. Electron backscattered diffraction (EBSD) was performed with a step size of 0.2 μm to determine the nature of the grains. The specimen for EBSD was polished by a JEOL IB-09020CP cross-section polisher for 3.5 h. The HKL Channel 5 software was used to further analyze the raw EBSD data. A high-resolution transmission electron microscope (HR-TEM) was applied to characterize the morphologies of grains

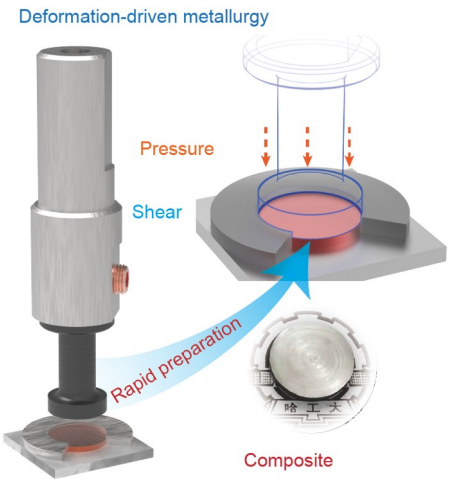

Figure 2 Schematic of the DDM process and the fabricated composites.

and dislocation distribution at a working voltage of 200 kV. The Al phase of the composites was investigated by an X-ray diffractometer (XRD). The XRD scanning range was set from 38° to 80° using a Cu Kα (λ = 0.1541 nm). An Instron 5569 tester was applied to test the tensile properties with a strain rate of 3.3 × 10^{-4} s^{-1} at room temperature. Three specimens were tested for each parameter.

RESULTS

Microstructural characterization and tensile properties

The prepared $SiC_{5np\text{-}5\mu p}$/Al has an obvious heterogeneous structure with fine and coarse grains separated *via* the designed strategy, as illustrated in Fig. 3a. The fine grains were pointed out by the inverse pole figure (IPF), and the coarse grains were selected by the band contrast figure (Fig. 3a). The IPF with the information of grain size and the grain orientation can also be found in Fig. S3. AMCs with typical heterogeneous structures could be obtained with the mixed SiC addition *via* DDM. During the tensile process, the coarse and fine grains underwent varying degrees of strain apparently. As shown in Fig. 3b, in the center field of the view, parabolic dimples (pointed out by blue lines) surrounded by the equiaxed dimples (demarcated by

 © Science China Press and Springer-Verlag GmbH Germany, part of Springer Nature 2022

yellow lines) were observed. The morphology features of dimples were only influenced by stress states. Parabolic dimples underwent the shear stress, while equiaxed dimples underwent the axial stress. Usually, the parabolic dimples were formed at the shear lips of the fracture surface macroscopically. The formation of mixed equiaxed-parabolic dimples with the micro-scale less than 20 μm in length indicated that the stress state was different in this micro-region. The strain incompatibility of the coarse and fine grains occurred, and the stress partitioning and strain transfer were procured during the deformation process. With such typical heterogeneous microstructures, the prepared $SiC_{5np\text{-}5\mu p}$/Al well balanced the strength and ductility. Fig. 4 shows the engineering stress/strain curves of the composites and summarizes the tensile properties of SiC-reinforced pure Al or Al alloys among other reported literature [6,25–34]. The SiC-reinforced AMCs obtained by our strategy exhibit the best strength-ductility synergy so far. The ultimate tensile strength and uniform elongation of the designed $SiC_{5np\text{-}5\mu p}$/Al composite reached 324 MPa and 12.9%, respectively, and the strength was 181% as high as that of the $SiC_{10\mu p}$/Al with only 3% ductility loss. Particularly notable is the uniform-elongation regime (removed the elastic strain from the uniform elongation), which indicates the work-hardening capacity of the samples and is usually used to evaluate the ductility. Compared with the $SiC_{10\mu p}$/Al, the yield strength of SiC_{10np}/Al was increased by 108 MPa with 73% uniform-elongation regime loss, while the yield strength of $SiC_{5np\text{-}5\mu p}$/Al was increased by 95 MPa with only 4% uniform-elongation regime loss. The $SiC_{5np\text{-}5\mu p}$/Al exhibited great strength-ductility synergy. Obviously, different from the SiC_{10np}/Al, the strength of $SiC_{5np\text{-}5\mu p}$/Al was not simply relying on mechanisms like Orowan strengthening. The strength improvement of the samples relying on these conventional mechanisms was usually at the expense of ductility loss. The typical heterogeneous microstructures of $SiC_{5np\text{-}5\mu p}$/Al must have played an important role during the strengthening process.

To further investigate the strength-ductility synergy phenomenon, the EBSD data of the $SiC_{10\mu p}$/Al were tested and set as the control group. With the nano-SiC particles mixed, the proportion of the fine grains (under 1.5 μm) in the $SiC_{5np\text{-}5\mu p}$/Al was increased by about 10% (Fig. 5) compared with that of the $SiC_{10\mu p}$/Al. The difference in the average grain diameter between the two AMCs was only about 0.3 μm, as shown in Fig. 5. The result declared that the nano-SiC particles did refine the part of the grains, but a large portion of the coarse grains was still maintained in the $SiC_{5np\text{-}5\mu p}$/Al. Thus, the grain size effect was not the main reason for the desirable strength-ductility synergy of the $SiC_{5np\text{-}5\mu p}$/Al. The EBSD data were further processed by the channel 5 software to give the GNDs distribution information of the $SiC_{5np\text{-}5\mu p}$/Al and $SiC_{10\mu p}$/Al, respectively. Under the same strain rate, the GNDs density of the $SiC_{5np\text{-}5\mu p}$/Al reached 5.20×10^{13} m^{-2}, which was about 31% larger than that of the $SiC_{10\mu p}$/Al (Fig. 5). The GNDs distribution maps of the $SiC_{5np\text{-}5\mu p}$/Al and $SiC_{10\mu p}$/Al were given in Fig. S4. The extra generated GNDs in the $SiC_{5np\text{-}5\mu p}$/Al indicated that its strain was not uniform. The deformation incompatibility occurred among the grains, which is consistent with the result shown in Fig. 3b. The Gaussian fit was conducted to the distribution of GNDs. The standard deviation of $SiC_{5np\text{-}5\mu p}$/Al was about 61% larger than

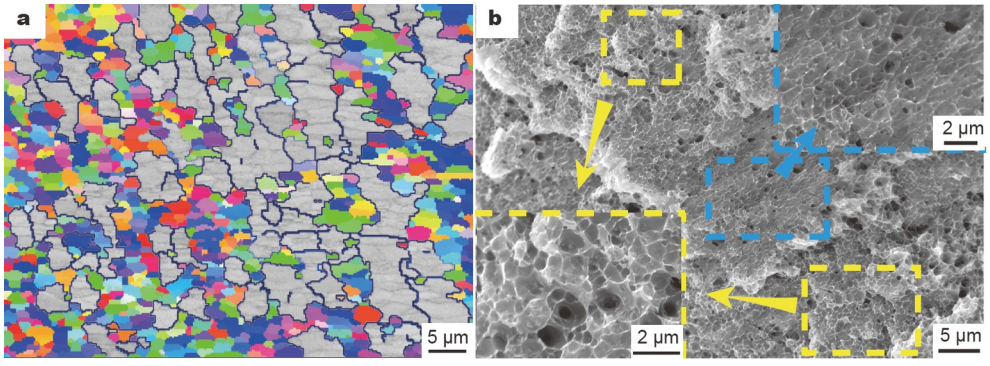

Figure 3 Microstructures of the $SiC_{5np\text{-}5\mu p}$/Al composites: (a) the IPF mixed with the band contrast figure; (b) the fracture morphology of $SiC_{5np\text{-}5\mu p}$/Al with mixed equiaxed-parabolic dimples.

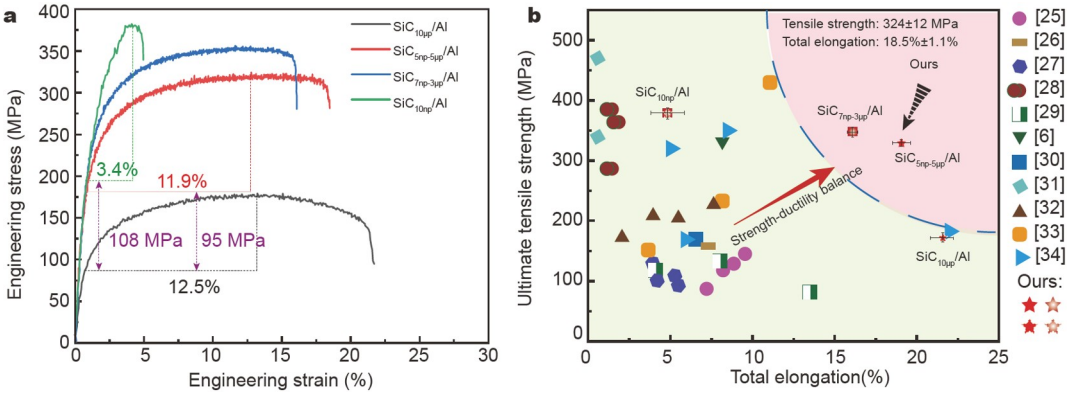

Figure 4 Tensile properties of the prepared AMCs: (a) the engineering stress/strain curves of the composites; (b) comparison of ultimate tensile strength *vs.* elongation achieved in the present work and the reported literature [6,25–34].

© Science China Press and Springer-Verlag GmbH Germany, part of Springer Nature 2022

that of $SiC_{10\mu p}$/Al, which means the GNDs distribution of $SiC_{5np\text{-}5\mu p}$/Al was less uniform. Such a result confirmed the heterostructure feature of $SiC_{5np\text{-}5\mu p}$/Al, which was considered as the key point determining the property of the designed AMCs.

Microstructural characterization and tensile properties

Fig. 6a, b depict the dispersion condition of SiC particles in $SiC_{10\mu p}$/Al and $SiC_{5np\text{-}5\mu p}$/Al. The mixed SiC particles containing nano-SiC and micro-SiC particles in $SiC_{5np\text{-}5\mu p}$/Al were observed. The nano-SiC particles had a slight aggregation tendency. The range of particle cluster size was from tens of nanometers to 200 nm approximately (Fig. 6d). The micro-SiC particles were broken slightly with the severe plastic deformation (Fig. 6c). The average size of micro-SiC particles was about 10 times larger than that of the nano-SiC particles. The size difference between the two particles made their distribution site diverse, which further influenced the dynamic recrystallization (DRX). The micro-SiC particles were distributed intergranularly, while the nano-SiC particles were intragranularly dispersed (Fig. 6c, d). More distribution features and the identification of SiC particles

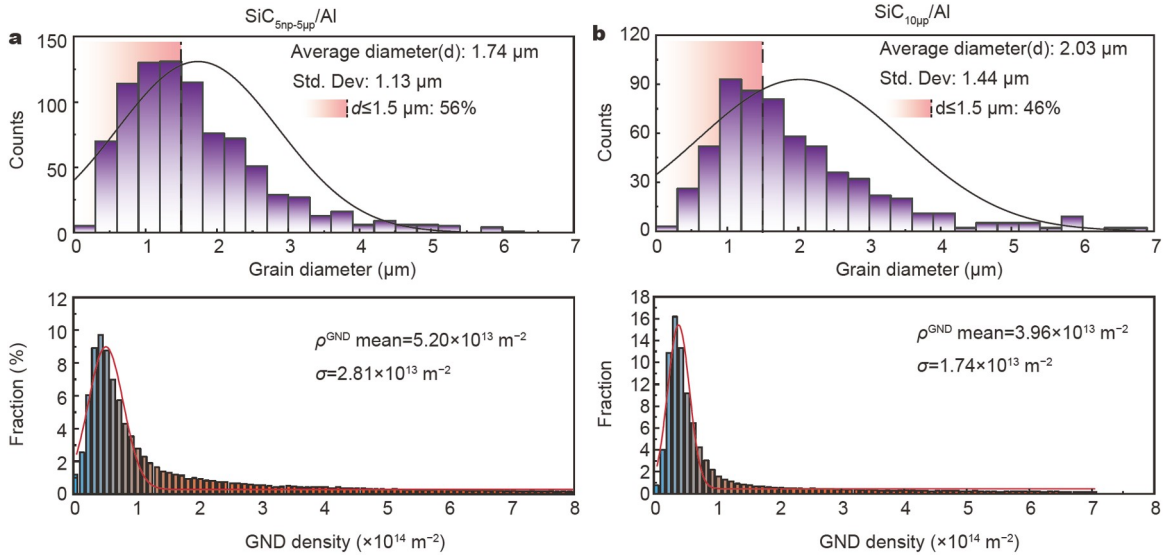

Figure 5 Grain diameter and GNDs density analysis of the $SiC_{5np\text{-}5\mu p}$/Al (a) and $SiC_{10\mu p}$/Al (b).

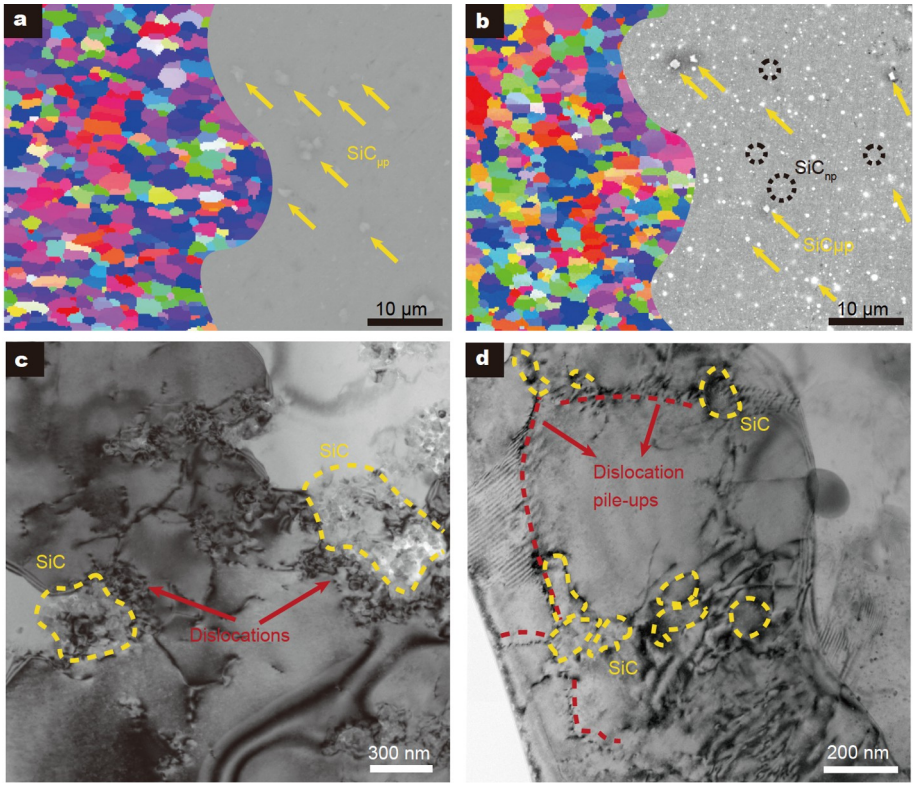

Figure 6 Typical dispersion of (a) micro-SiC particles in $SiC_{10\mu p}$/Al and (b) mixed SiC particles in $SiC_{5np\text{-}5\mu p}$/Al; the distribution of micro-SiC particles (c) and nano-SiC particles (d) in $SiC_{5np\text{-}5\mu p}$/Al.

© Science China Press and Springer-Verlag GmbH Germany, part of Springer Nature 2022

were introduced in Figs S5–S8.

The refinement of Al, as the material with high stacking fault energies, was mainly caused by dislocation accumulation and rearrangement. During the DDM process, the dislocations produced around the micro-SiC particles (Fig. 6c), served as the preferable sites for crystallization nucleation. Only the DRX process adjacent to the particle was promoted, known as the particle-stimulated nucleation mechanism [35,36]. As dispersed inside the grains, the nano-SiC particles hindered the further slide of dislocations. The dislocation interaction was promoted with the deformation stress accumulated, which accelerated the pile-up of dislocations (Fig. 6d). These dislocation pile-ups may turn into new grain boundaries with further evolution of the microstructure. Some of the nano-SiC particles pinned at the dislocation pile-ups (Fig. 6d) may be still retained at the newly formed grain boundaries and hindered their further movement. The grains in the $SiC_{5np\text{-}5\mu p}$/Al were thus further refined. Apparently, the nano-SiC particles had a better grain refinement capacity compared with the micro-SiC particles. These different capabilities to refine the grains induced the heterogeneous structure in the $SiC_{5np\text{-}5\mu p}$/Al. Moreover, benefiting from the characteristics of the DDM method, such as short-time preparation, severe plastic deformation, solid-phase method, and high recrystallization tendency, the influence of different-sized SiC particles on the matrix grains was magnified. Such a heterostructure may be challenging to obtain in other methods.

DISCUSSION

Stress and GNDs state between coarse/fine grains

Fig. 7a depicts the DRX of $SiC_{5np\text{-}5\mu p}$/Al during the DDM process. As pointed out by the black dot line, a large elongated grain containing several minor grains was observed. The high angle grain boundaries (HAGBs) migrated to form serrations, which were considered the typical feature of geometric DRX. Along with direction A (Fig. 7a), three selected minor grains in the large elongated grains were tested. As shown in Fig. 7c, the three adjacent grains have diverse lattice orientations. With gradual lattice rotation near HAGBs, the DRX process was promoted, which was generally acknowledged as the continuous DRX process. The large strain rate of the DDM process provided a sufficient driving force to enable the coexistence of multiple recrystallization mechanisms, which increased the recrystallization tendency of the composites.

The distribution of GNDs among the coarse and fine grains is shown in Fig. 7b. The high-density sites (the red/yellow sites in Fig. 7b) of the GNDs were nearly all produced close to the grain boundaries in the coarse grains. During the deformation process, the coarse and fine grains had different dislocation storabilities, which represent different deformabilities. GNDs were thus generated in the coarse grains to accommodate the deformation incompatibility. With the continuous generation of GNDs in the coarse grains, the strength of such sites adjacent to grain boundaries was improved. As illustrated in Fig. 7b, the soft-hard interface between coarse-fine grains thus migrated into the interior of coarse grains, which guaranteed the further generation of strains, as the inner part of the coarse grains provided enough space for the dislocations to glide. The ductility of the composites was thus promoted. As pointed out by the white line in grain B (Fig. 7b), a linear region with a high density of GNDs was observed. Such a region was not the stable grain boundaries, as the line profile test was conducted, and the misorientation

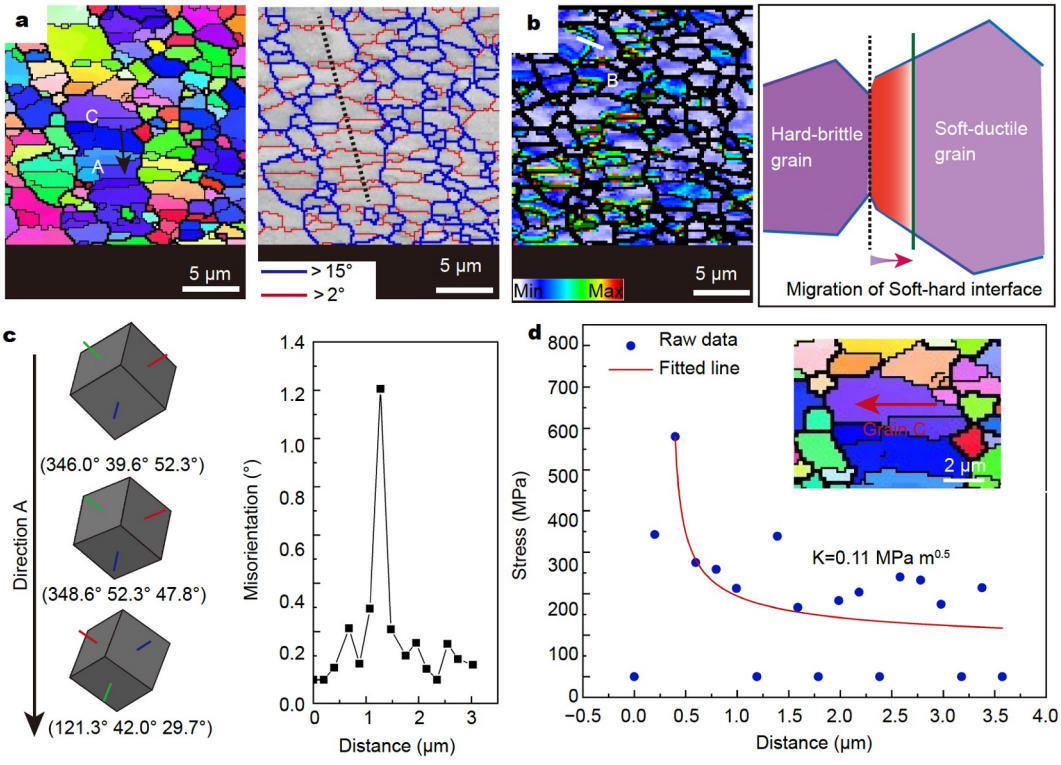

Figure 7 EBSD analysis of the $SiC_{5np\text{-}5\mu p}$/Al composites: (a) the IPF and the grain boundaries map; (b) the GNDs distribution and the schematic of the soft-hard interface migration; (c) the lattice rotation along direction A and the misorientation change along line B; (d) the fitted line of the intracrystalline stress along the red arrow in grain C.

 © Science China Press and Springer-Verlag GmbH Germany, part of Springer Nature 2022

was confirmed as about 1.2° (Fig. 7c). Such a phenomenon indicated that under the severe plastic deformation of DDM, the GNDs in the coarse grains have a sufficient driving force to glide through the coarse grains.

The typical grain C (Fig. 7a, d) was selected to investigate the stress condition inside the coarse grains, which was surrounded by several fine grains. The stress σ was calculated by the following equation [37]:

$$\sigma = M\alpha Gb\rho^{0.5}, \tag{1}$$

where M = 3.06 is the Taylor factor, α = 0.2 is a constant for dislocation strengthening for Al, G = 25.4 GPa is the shear modulus of the Al matrix, b is the Burger vector and taking 0.286 nm for Al, and ρ is the dislocation density and was estimated using the strain-gradient-based model [18,37]:

$$\rho = \frac{2\theta}{ub}, \tag{2}$$

where θ is the misorientation angle, and u is the step size used in EBSD analysis.

Along the direction pointed out by the red arrow in grain C (Fig. 7d), the flow stress was tested and calculated. The raw data are shown in Fig. 7d (blue dots) and fitted to the following model (red line in Fig. 7d) [38]:

$$\tau = A + \frac{K}{\sqrt{X+B}}, \tag{3}$$

where τ is the flow stress inside the grain, the constant K is the stress intensity factor, and X is the distance. Parameters A and B are included to allow for uncertainty in the grain boundary position and far-field elastic strain state [39].

As shown in Fig. 7d, a stress field directed from the grain boundary to the intracrystalline side was formed inside the coarse grains, which was caused by the accumulation of GNDs. The stress field is consistent with the analysis of Fig. 7b. Moreover, the stress intensity factor K was calculated as 0.11 MPa m$^{0.5}$ in the selected coarse grain C, which was higher than the common value (0.07 MPa m$^{0.5}$) for Al. The result indicated that the pile-ups of GNDs close to the grain boundaries induced extra stress compared with the model used in the conventional homogeneous materials. Such extra strengthening effect induced by the GNDs was usually considered as back stress strengthening.

Evaluation of back stress *via* three basal mechanisms

The value of back stress was evaluated by the value-difference between the experimentally tested yield strength and the sum of the three strengthening mechanisms (Orowan strengthening, grain size strengthening, and dislocation strengthening). During the DDM process, the micro-SiC particles were broken, and the nano-SiC particles were agglomerated slightly. Observed by the TEM and SEM, the mean radius of the particles was counted as 824 nm statistically. According to the Orowan strengthening theory, the yield strength increased by the SiC particles can be calculated using the following equation [40]:

$$\Delta\sigma_{\mathrm{or}} = M\frac{0.4Gb}{\pi\sqrt{1-\nu}}\frac{\ln(\frac{2r}{b})}{L}, \tag{4}$$

where ν = 0.35 is the Poisson's ratio of pure Al matrix, r is the mean radius of the particles, and L is the average inter-particle spacing and is calculated by the equation [41]:

$$L = r\left[\left(\frac{2\pi}{3f}\right)^{0.5} - 2\left(\frac{2\pi}{3}\right)^{0.5}\right], \tag{5}$$

where f is the volume fraction of the particles.

The value of the grain size strengthening was estimated by the Hall-Petch relationship [42–44]:

$$\Delta\sigma_{\mathrm{G}} = K\left(d^{-0.5} - d_0^{-0.5}\right) \approx Kd^{-0.5}, \tag{6}$$

where K is a constant (0.07 MPa m$^{0.5}$ for Al), d_0 = 300–400 μm is the reference coarse grain size of pure Al, d is the average grain size of the AMCs calculated by EBSD. The value of $d_0^{-0.5}$ is much smaller than that of the $d^{-0.5}$, which can be ignored to simplify the calculation.

The contribution of the dislocation was calculated by Equation (1). The density of the dislocation used in Equation (1) was estimated *via* the Williamson-Hall method, as follows [45]:

$$\beta_{hkl}\cos\theta = \frac{0.94\lambda}{D} + 4\varepsilon\sin\theta, \tag{7}$$

where β_{hkl} is the full width at the half-maximum intensity of the selected peak in degrees (rad), which is calculated by the equation [46]:

$$\beta_{hkl} = \left(\beta_{hkl\,\mathrm{M}}^{\ 2} - \beta_{hkl\,\mathrm{In}}^{\ 2}\right)^{0.5}, \tag{8}$$

where $\beta_{hkl\,\mathrm{M}}$ and $\beta_{hkl\,\mathrm{In}}$ are the observed and instrumental peak broadening, respectively.

The density of the dislocation was calculated by [46]

$$\rho = \frac{2\sqrt{3}(\varepsilon^2)^{0.5}}{Db}, \tag{9}$$

where D and ε are the crystallite size and microstrain, respectively. λ is the wavelength of Cu-Kα radiation (λ = 0.1541 nm).

The five XRD peaks of Al were tested and processed *via* Equations (7)–(9). The results are shown in Fig. 8a. Another method to evaluate the dislocation density was also conducted to ensure the accuracy of the data (illustrated in Table S2). As illustrated in Fig. 8c, the yield strength *via* experiment was about 65 MPa higher than the sum of the three calculated strengthening mechanisms.

It can be attributed to the following reasons: (a) the statistically stored dislocation and the GNDs were treated to have the same contribution to the strengthening effect, which cannot be ignored in heterogeneous materials. (b) As shown in Fig. 7d, the stress intensity factor K was much higher than the common value (0.07 MPa m$^{0.5}$) for Al, which indicated that the additional strengthening occurred around the grain boundaries. Such extra strengthening effect was also reported in another aspect that the hardening in the grain boundary region was higher when a Taylor 'soft' grain was adjacent to a Taylor 'hard' grain [47], which was also observed in the present research (Fig. 8b). Apparently, the accumulated GNDs did have a great contribution to the extra-strengthening while accommodating the incompatible deformation among coarse-fine grains.

Strength-ductility synergy mechanism

Fig. 9a, b depict the typical pile-ups of dislocations. The dislocations were generated to accommodate the deformation incompatibility between the coarse and fine grains under the applied stress. The dislocation resource was assumed at point X, as shown in Fig. 10a. As the dislocations glide forward, the plastic strain was produced, and each dislocation left a displacement of one Burgers vector in its wake. The accumulated strain is illustrated in Fig. 10b. The strain was zero at the grain boundary, and the max strain was performed at the dislocation

 © Science China Press and Springer-Verlag GmbH Germany, part of Springer Nature 2022

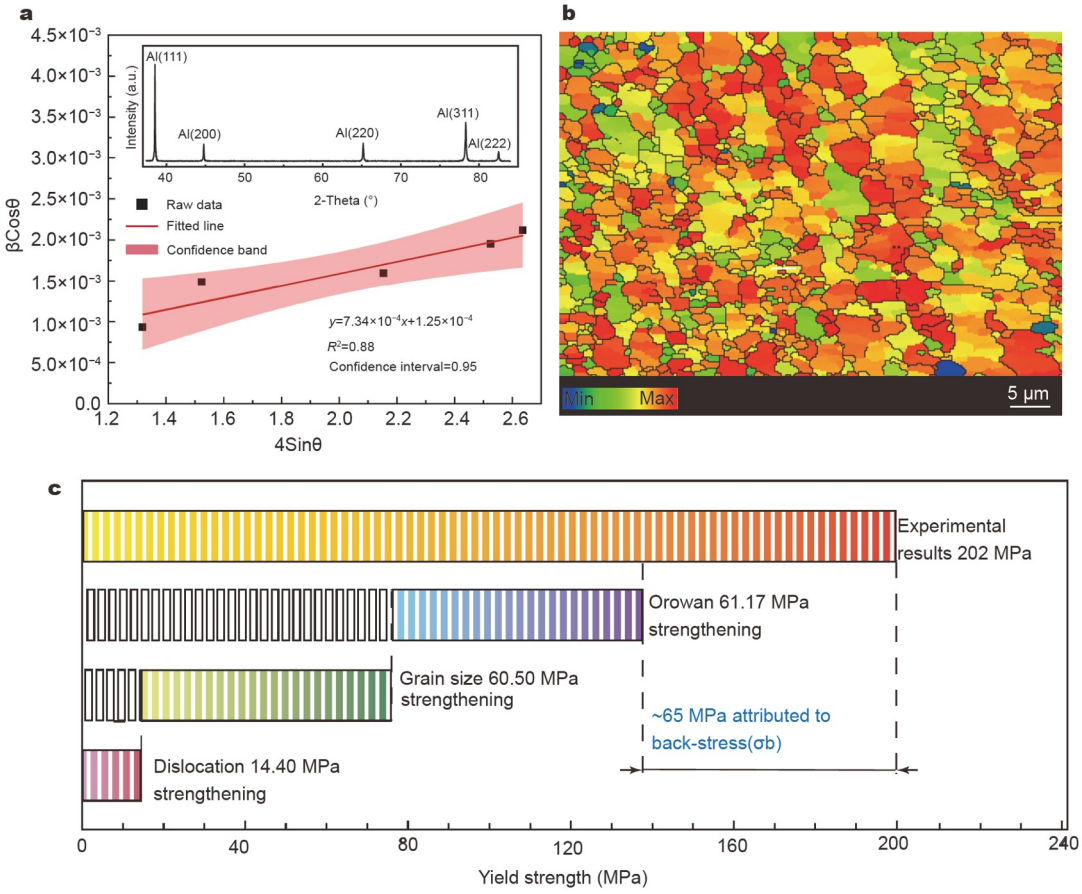

Figure 8 Analysis of the strengthening mechanism of $SiC_{5np\text{-}5\mu p}$/Al composites: (a) the Williamson-Hall method to estimate the dislocation density; (b) the Taylor factor distribution and (c) the comparison of the theoretically calculated value with the experimental results.

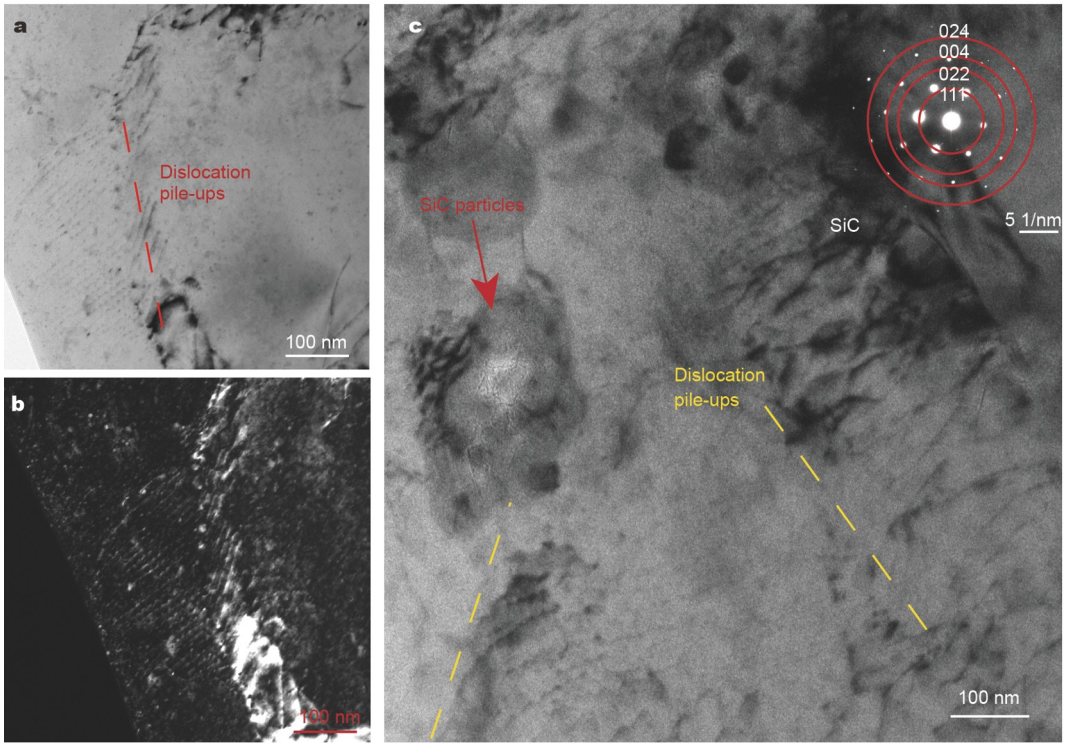

Figure 9 The two main types of dislocation pile-ups in the $SiC_{5np\text{-}5\mu p}$/Al: (a) the dislocation pile-ups, and (b) the corresponding dark field image; (c) the interaction of the nano-SiC particles and dislocation pile-ups.

 © Science China Press and Springer-Verlag GmbH Germany, part of Springer Nature 2022

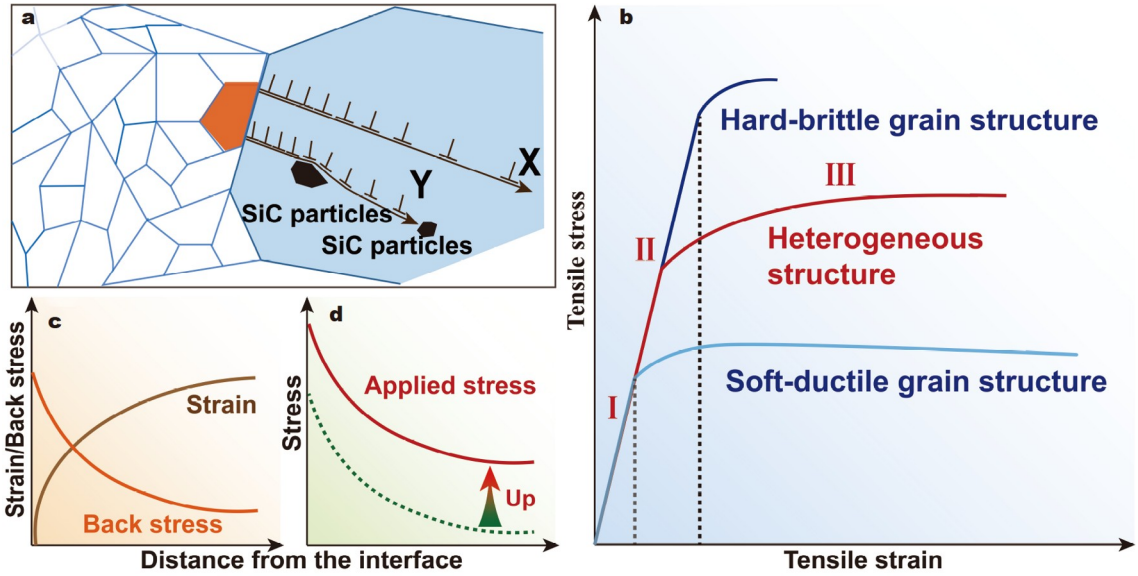

Figure 10 Schematics of the strength-ductility synergy mechanisms: (a) the interaction of the nano-SiC particles between GNDs; (b) the change of the strain and back stress along the distance from the grain boundary; (c) the increased applied stress; (d) the deformation stages of the heterogeneous materials.

source X. With the continued applied stress (τ_b), the dislocations would pile up at the grain boundary, and the responding back stress (τ_b) would generate. The stress gradient was illustrated by the red curve shown in Fig. 10b. The back stress induced by the pile-up dislocations balanced the applied stress and made the system reach equilibrium. The effective stress derived from the dislocation at the source X can be expressed as the following equation [17]:

$$\tau_e = \tau_a - \tau_b. \quad (10)$$

The further movement of the dislocation needed the higher-stress effect, which meant the higher applied stress. Simultaneously, the back stress would also be increased with the further pile-up of dislocations. Thus, back stress was a long-range stress that maintained the dynamic balance with the applied stress. Such a dynamic balance procedure ensured the strength-ductility synergized improvement of the heterostructure.

As shown in Fig. 9c, the interaction of the intragranularly dispersed SiC particles with pile-up dislocations was observed. The local stress gradient caused by the nano-SiC particles would hinder the movement of the dislocation, which thereby increased the back stress. To balance this stress, more applied stress was needed. Thus, the strengthening effect was further promoted under the coupling of the heterostructure and the intragranularly dispersed SiC particles, as illustrated by Fig. 10c.

The deformation process of the heterostructure was classified into three stages in Fig. 10d. In stage I, the soft-ductile grains and the hard-brittle grains deformed elastically. In stage II, with more applied stress, the soft-ductile grains began to deform plastically, while the hard-brittle grains still maintained the elastic deformation. This stage was particularly important, as equilibrium was kept by the back stress and the applied stress occurred in this stage, which determined the strength-ductility synergy of the designed heterostructure. The intragranular dispersion of nano-SiC particles was designed to extend this stage. At this stage, the densities of GNDs in the coarse grains were increased. With elastically and plastically deformed grains at the same stage (stage II), the strengthening process was not linear with the strain gradient, which was considered to be the feature of the heterogeneous structure theoretically. Such similar results were reported by Wang *et al.* [48] in another respect. In stage III, the soft-ductile grains were hardened by the GNDs, which had almost the same strength as the hard-brittle grains, and then deformed plastically together. Among the above three stages, the soft-ductile grains sustained more strain than the hard-brittle grains, which produced the strain partitioning, as discussed in Figs 3b and 7b.

CONCLUSIONS

A heterogeneous grain structure induced by the mixed distribution of SiC particles was achieved *via* DDM. The heterogeneous microstructural evolution and the back stress-enabled strength-ductility synergy mechanism were revealed.

(1) The back stress was increased by the accumulated GNDs and the intragranularly dispersed SiC particles simultaneously. As a long-range stress, the back stress maintained the dynamic balance with the applied stress, which was the key point to ensuring the strength-ductility synergized improvement.

(2) The formation of a typical heterogeneous structure was induced by the difference in the capacity to refine the grains between micro-SiC and nano-SiC particles. The GNDs were generated in the coarse grains to accommodate the deformation incompatibility in the heterostructures, which has extra hardening in the grain boundary region.

(3) The ultimate tensile strength and uniform elongation of the designed $SiC_{5np\text{-}5\mu p}$/Al composite reached 324 MPa and 12.9%, respectively, and the strength was 181% as high as that of the $SiC_{10\mu p}$/Al with only 3% ductility loss.

The strength-ductility synergy of the AMCs could be enhanced effectively through the back stress engineering with the interface designing of coarse-fine grains and the reinforcements of intragranular-dispersed tailoring.

Received 29 July 2022; accepted 26 September 2022; published online 14 December 2022

 © Science China Press and Springer-Verlag GmbH Germany, part of Springer Nature 2022

1 Zhang Q, Xiao BL, Wang WG, *et al.* Reactive mechanism and mechanical properties of *in situ* composites fabricated from an Al-TiO_2 system by friction stir processing. Acta Mater, 2012, 60: 7090–7103
2 Su Y, Li Z, Yu Y, *et al.* Composite structural modeling and tensile mechanical behavior of graphene reinforced metal matrix composites. Sci China Mater, 2018, 61: 112–124
3 Xie Y, Meng X, Chang Y, *et al.* Ameliorating strength-ductility efficiency of graphene nanoplatelet-reinforced aluminum composites *via* deformation-driven metallurgy. Compos Sci Tech, 2022, 219: 109225
4 Jiang J, Chen G, Wang Y. Compression mechanical behaviour of 7075 aluminium matrix composite reinforced with nano-sized SiC particles in semisolid state. J Mater Sci Tech, 2016, 32: 1197–1203
5 Li X, Liu C, Luo K, *et al.* Hot deformation behaviour of SiC/AA6061 composites prepared by spark plasma sintering. J Mater Sci Tech, 2016, 32: 291–297
6 Jiang W, Zhu J, Li G, *et al.* Enhanced mechanical properties of 6082 aluminum alloy *via* SiC addition combined with squeeze casting. J Mater Sci Tech, 2021, 88: 119–131
7 Tariq NH, Gyansah L, Qiu X, *et al.* Achieving strength-ductility synergy in cold spray additively manufactured Al/B4C composites through a hybrid post-deposition treatment. J Mater Sci Tech, 2019, 35: 1053–1063
8 Xie Y, Meng X, Chang Y, *et al.* Heteroatom modification enhances corrosion durability in high-mechanical-performance graphene-reinforced aluminum matrix composites. Adv Sci, 2022, 9: 2104464
9 Xie Y, Meng X, Li Y, *et al.* Insight into ultra-refined grains of aluminum matrix composites *via* deformation-driven metallurgy. Compos Commun, 2021, 26: 100776
10 Dong S, Zhou J, Hui D, *et al.* Size dependent strengthening mechanisms in carbon nanotube reinforced metal matrix composites. Compos Part A-Appl Sci Manufacturing, 2015, 68: 356–364
11 Wu X, Yang M, Li R, *et al.* Plastic accommodation during tensile deformation of gradient structure. Sci China Mater, 2021, 64: 1534–1544
12 Luo S, Su Y, Wang Z. Tailored microstructures and strengthening mechanisms in an additively manufactured dual-phase high-entropy alloy *via* selective laser melting. Sci China Mater, 2020, 63: 1279–1290
13 Xie Y, Meng X, Mao D, *et al.* Homogeneously dispersed graphene nanoplatelets as long-term corrosion inhibitors for aluminum matrix composites. ACS Appl Mater Interfaces, 2021, 13: 32161–32174
14 Gao P, Ma Z, Gu J, *et al.* Exceptional high-strain-rate tensile mechanical properties in a CrCoNi medium-entropy alloy. Sci China Mater, 2022, 65: 811–819
15 Han BO, Lavernia EJ, Lee Z, *et al.* Deformation behavior of bimodal nanostructured 5083 Al alloys. Metall Mat Trans A, 2005, 36: 957–965
16 Wu X, Yang M, Yuan F, *et al.* Heterogeneous lamella structure unites ultrafine-grain strength with coarse-grain ductility. Proc Natl Acad Sci USA, 2015, 112: 14501–14505
17 Wu X, Zhu Y. Heterogeneous materials: A new class of materials with unprecedented mechanical properties. Mater Res Lett, 2017, 5: 527–532
18 Ma X, Huang C, Moering J, *et al.* Mechanical properties of copper/bronze laminates: Role of interfaces. Acta Mater, 2016, 116: 43–52
19 Li D, Fan G, Huang X, *et al.* Enhanced strength in pure Ti *via* design of alternating coarse- and fine-grain layers. Acta Mater, 2021, 206: 116627
20 Zhang Z, Vajpai SK, Orlov D, *et al.* Improvement of mechanical properties in SUS304L steel through the control of bimodal microstructure characteristics. Mater Sci Eng-A, 2014, 598: 106–113
21 Lu K. Making strong nanomaterials ductile with gradients. Science, 2014, 345: 1455–1456
22 Wang J, Ferdowsi MRG, Lynch PA, *et al.* Influence of precipitation on tension and compression twinning in Mg-6.5Zn alloy. Scripta Mater, 2022, 207: 114253
23 Bhattacharyya JJ, Bittmann B, Agnew SR. The effect of precipitate-induced backstresses on plastic anisotropy: Demonstrated by modeling the behavior of aluminum alloy, 7085. Int J Plast, 2019, 117: 3–20
24 Keller C, Hug E, Feaugas X. Microstructural size effects on mechanical properties of high purity nickel. Int J Plast, 2011, 27: 635–654
25 Song M, He Y. Effects of die-pressing pressure and extrusion on the microstructures and mechanical properties of SiC reinforced pure aluminum composites. Mater Des, 2010, 31: 985–989
26 Reddy MP, Shakoor RA, Parande G, *et al.* Enhanced performance of nano-sized SiC reinforced Al metal matrix nanocomposites synthesized through microwave sintering and hot extrusion techniques. Prog Nat Sci-Mater Int, 2017, 27: 606–614
27 Sun C, Song M, Wang Z, *et al.* Effect of particle size on the microstructures and mechanical properties of SiC-reinforced pure aluminum composites. J Materi Eng Perform, 2011, 20: 1606–1612
28 Xin L, Yang W, Zhao Q, *et al.* Strengthening behavior in SiC nanowires reinforced pure Al composite. J Alloys Compd, 2017, 695: 2406–2412
29 Soltani S, Azari Khosroshahi R, Taherzadeh Mousavian R, *et al.* Stir casting process for manufacture of Al-SiC composites. Rare Met, 2017, 36: 581–590
30 Karakizis PN, Pantelis DI, Fourlaris G, *et al.* Effect of SiC and TiC nanoparticle reinforcement on the microstructure, microhardness, and tensile performance of AA6082-T6 friction stir welds. Int J Adv Manuf Technol, 2018, 95: 3823–3837
31 Xiu Z, Yang W, Dong R, *et al.* Microstructure and mechanical properties of 45 vol.% SiCp/7075Al composite. J Mater Sci Tech, 2015, 31: 930–934
32 Dong P, Zhao H, Chen F, *et al.* Microstructures and properties of A356-10%SiC particle composite castings at different solidification pressures. Trans Nonferrous Met Soc China, 2013, 23: 2222–2228
33 Boostani AF, Mousavian RT, Tahamtan S, *et al.* Graphene sheets encapsulating SiC nanoparticles: A roadmap towards enhancing tensile ductility of metal matrix composites. Mater Sci Eng-A, 2015, 648: 92–103
34 Zhu J, Jiang W, Li G, *et al.* Microstructure and mechanical properties of SiC_{np}/Al6082 aluminum matrix composites prepared by squeeze casting combined with stir casting. J Mater Processing Tech, 2020, 283: 116699
35 Wang XY, Jiang JT, Li GA, *et al.* Particle-stimulated nucleation and recrystallization texture initiated by coarsened Al_2CuLi phase in Al-Cu-Li alloy. J Mater Res Tech, 2021, 10: 643–650
36 Huo W, Hou L, Cui H, *et al.* Fine-grained AA 7075 processed by different thermo-mechanical processings. Mater Sci Eng-A, 2014, 618: 244–253
37 Choi SW, Won JW, Lee S, *et al.* Deformation twinning activity and twin structure development of pure titanium at cryogenic temperature. Mater Sci Eng-A, 2018, 738: 75–80
38 Guo Y, Britton TB, Wilkinson AJ. Slip band-grain boundary interactions in commercial-purity titanium. Acta Mater, 2014, 76: 1–12
39 Benjamin Britton T, Wilkinson AJ. Stress fields and geometrically necessary dislocation density distributions near the head of a blocked slip band. Acta Mater, 2012, 60: 5773–5782
40 Wang X, Guan RG, Misra RDK, *et al.* The mechanistic contribution of nanosized Al_3Fe phase on the mechanical properties of Al-Fe alloy. Mater Sci Eng-A, 2018, 724: 452–460
41 Ferguson JB, Lopez H, Kongshaug D, *et al.* Revised Orowan srengthening: Effective interparticle spacing and strain field considerations. Metall Mat Trans A, 2012, 43: 2110–2115
42 Chen B, Kondoh K, Li JS, *et al.* Extraordinary reinforcing effect of carbon nanotubes in aluminium matrix composites assisted by *in-situ* alumina nanoparticles. Compos Part B-Eng, 2020, 183: 107691
43 Huang Y, Li J, Wan L, *et al.* Strengthening and toughening mechanisms of CNTs/Mg-6Zn composites *via* friction stir processing. Mater Sci Eng-A, 2018, 732: 205–211
44 Mao D, Meng X, Xie Y, *et al.* Strength-ductility balance strategy in SiC reinforced aluminum matrix composites *via* deformation-driven metallurgy. J Alloys Compd, 2022, 891: 162078
45 Khorsand Zak A, Abd. Majid WH, Abrishami ME, *et al.* X-ray analysis of ZnO nanoparticles by Williamson-Hall and size-strain plot methods. Solid State Sci, 2011, 13: 251–256
46 Baghdadi AH, Rajabi A, Selamat NFM, *et al.* Effect of post-weld heat treatment on the mechanical behavior and dislocation density of friction stir welded Al6061. Mater Sci Eng-A, 2019, 754: 728–734
47 Vachhani SJ, Doherty RD, Kalidindi SR. Studies of grain boundary regions in deformed polycrystalline aluminum using spherical nanoindentation. Int J Plast, 2016, 81: 87–101
48 Wang YF, Huang CX, Fang XT, *et al.* Hetero-deformation induced (HDI) hardening does not increase linearly with strain gradient. Scripta

 © Science China Press and Springer-Verlag GmbH Germany, part of Springer Nature 2022

Mater, 2020, 174: 19–23

Acknowledgements The work was jointly supported by China National Postdoctoral Program for Innovative Talents (BX20220384), the National Natural Science Foundation of China (52175301), the Natural Science Foundation of Heilongjiang Province (JJ2020JQ085), and China Postdoctoral Science Foundation (2021T140151).

Author contributions Mao D performed the experiments and wrote the paper; Meng X and Xie Y contributed to the theoretical analysis; Chang Y, Qin Z, Xu S, and Wan L performed part of the experiments and reviewed the paper; Huang Y conceived the concept and supervised this study. All authors contributed to the general discussion.

Conflict of interest The authors declare that they have no conflict of interest.

Supplementary information Supporting data are available in the online version of the paper.

Dongxin Mao received his Master's degree from Harbin University of Science and Technology in 2020. Currently, he is a PhD candidate at the State Key Laboratory of Advanced Welding and Joining, Harbin Institute of Technology, China. His current research interest focuses on the friction stir welding and deformation-driven metallurgy of aluminum matrix composites.

Xiangchen Meng received his PhD degree from Harbin Institute of Technology in 2020. Currently, he is an associate research fellow at the State Key Laboratory of Advanced Welding and Joining, Harbin Institute of Technology, China. His current research interest focuses on friction stir welding and metal matrix composites.

Yuming Xie received his PhD degree from Harbin Institute of Technology in 2022. Currently, he is an assistant professor at the State Key Laboratory of Advanced Welding and Joining, Harbin Institute of Technology, China. His current research interest focuses on deformation-driven metallurgy: mechanical performances and anti-corrosion design, numerical modeling of friction-based techniques, friction-based welding and joining of organic materials and composites, and solid-state electrolytes and their applications in batteries.

Yongxian Huang received his PhD degree from Harbin Institute of Technology in 2008. Currently, he is a professor at the State Key Laboratory of Advanced Welding and Joining, Harbin Institute of Technology, China. His current research interest focuses on deformation-driven metallurgy: mechanical performances and anti-corrosion design, numerical modeling of friction-based techniques, friction-based welding and joining of organic materials and composites, and solid-state electrolytes and their applications in batteries.

背应力平衡策略实现非均质Al-SiC复合材料的强塑性协同

冒冬鑫[1†], 孟祥晨[1,2†], 谢聿铭[1,2†], 常月鑫[1], 秦志伟[1], 许双明[3], 万龙[1], 黄永宪[1,2*]

摘要 高强复合材料的低位错存储性能及其引发的强塑倒置问题阻碍了该系列材料的进一步发展. 本文通过新颖的形变驱动冶金方法, 设计了一种巧妙的具有粗细晶粒异质结构的纳微混合SiC增强铝基复合材料. 基于背应力理论对累积的几何必须位错和晶内分散的SiC颗粒进行调控, 使得背应力与外在施加应力保持动态平衡. 这是本策略实现材料强塑性协同的关键. 所设计的$SiC_{5np\text{-}5\mu p}$/Al复合材料的极限抗拉强度和均匀伸长率分别为324 MPa和12.9%, 达到$SiC_{10\mu p}$/Al抗拉强度的181%, 而塑性仅损失了约3%. 因此, 本文提供了一种基于背应力优化的强度-塑性协同新策略.

 © Science China Press and Springer-Verlag GmbH Germany, part of Springer Nature 2022